Soft Matter



PAPER View Article Online



Cite this: DOI: 10.1039/c9sm00016

Symmetries in hard polygon systems determine plastic colloidal crystal mesophases in two dimensions

Wenbo Shen,^a James Antonaglia, ^b Joshua A. Anderson,^b Michael Engel,†^b Greg van Anders [‡] and Sharon C. Glotzer ^b**

Orientational ordering is a necessary step in the crystallization of molecules and anisotropic colloids. Plastic crystals, which are possible mesophases between the fluid and fully ordered crystal, are translationally ordered but exhibit no long range orientational order. Here, we study the two-dimensional phase behavior of hard regular polygons with edge number n = 3-12. This family of particles provides a model system to isolate the effect of shape and symmetry on the existence of plastic crystal phases. We show that the symmetry group of the particle, G, and the symmetry group of the local environment in the crystal, H, together determine plastic colloidal crystal phase behavior in two dimensions. If G contains completely the symmetry elements of H, then a plastic crystal phase is absent. If G and H share some but not all nontrivial symmetry elements, then a plastic crystal phase exists with preferred particle orientations that recover the absent symmetry elements of the crystal; we call this phase the discrete plastic crystal phase. If G and H share no nontrivial symmetry elements, then a plastic crystal phase exists without preferred orientations, which we call an indiscrete plastic crystal.

Received 4th January 2019, Accepted 12th February 2019

DOI: 10.1039/c9sm00016j

rsc.li/soft-matter-journal

Entropy maximization in hard particle systems can lead to ordered phases such as plastic crystals, liquid crystals, and crystals. ¹⁻³ Like liquid crystals, plastic crystals are mesophases appearing in some systems between disordered fluids and ordered crystals. ¹ Whereas liquid crystals can exhibit long-range orientational order without translational order, plastic crystals exhibit translational order without long-range orientational order. Plastic crystals have been observed both in experiments ⁴⁻⁸ and computer simulations. ⁹⁻¹⁵ Yet despite their abundance, much less is known about plastic crystals than about liquid crystals, and their practical potential has yet to be fully realized. Understanding the conditions under which plastic crystals are to be expected would be useful in designing molecules or nanoparticles to achieve targeted materials with desired features or behavior. ^{16,17} One such example is the organic ionic plastic crystals (OIPCs) proposed for use in solid state

The appearance of plastic crystal phases has been ascribed to the tendency of particles to orient themselves to be compatible with their local environment.²³⁻²⁸ Here we show that compatibility is achieved for plastic crystal phases of hard shapes by matching symmetries to maximize entropy. In systems of hard polyhedra, entropy maximization is typically achieved via facet alignment; 1,2,29 particles sacrifice rotational entropy to gain translational entropy.²⁹ Likewise, hard polygon systems can maximize entropy by aligning their edges.30-35 We study hard regular polygons as a model system to isolate shape as the sole factor in producing a plastic crystal phase. We find that 3-, 4-, 6-, and 12-sided polygons self-assemble an orientationally-ordered crystal and no other translationally ordered mesophase; 5-, 7-, and 11-sided polygons exhibit a plastic crystal phase intermediate between the orientationally ordered crystal and the fluid; and 8-, 9-, and 10-sided polygons exhibit a partially orientationally-disordered plastic crystal mesophase. Taken together, our findings indicate that the ability for such systems to maximize edge alignment depends on both the particle symmetry and the symmetry group of the local environment in the solid phase.

electrochemical devices such as fuel cells and solar cells.¹⁸ There, molecular rotation leads to the formation of lattice defects, such as vacancies and dislocations.^{19–22} The presence of these defects is critical in creating empty sites to host moving ions and contributes to ion conductivity. Design rules for selecting organic molecules to achieve specific patterns of rotational motion in OIPCs could assist in maximizing ion conductivity.

^a Department of Physics, University of Michigan, Ann Arbor, Michigan 48109, USA. E-mail: sglotzer@umich.edu

^b Department of Chemical Engineering, University of Michigan, Ann Arbor, Michigan 48109, USA

^c Department of Materials Science & Engineering, University of Michigan, Ann Arbor, Michigan 48109, USA

^d Biointerfaces Institute, University of Michigan, Ann Arbor, Michigan 48109, USA

[†] Current address: Institute for Multiscale Simulation, Friedrich-Alexander-Universität Erlangen-Nürnberg, 91052 Erlangen, DE, Germany.

[‡] Current address: Department of Physics, Engineering Physics and Astronomy, Queen's University, Kingston, Ontario, CA, K7L 3N6, Canada.

Paper Soft Matter

By quantifying the strength of directional entropic forces, ^{17,36,37} we show that if the particle symmetry group contains completely the symmetry elements of the local environment, then a plastic crystal phase is absent. If the particle and local environment share some but not all nontrivial symmetry elements (symmetry elements besides the identity operation), then a "discrete" plastic crystal phase exists with preferred particle orientations that recover the absent symmetry elements of the solid. If they share no nontrivial symmetry elements, then an "indiscrete" plastic crystal phase exists without preferred orientations.

Model and methods

We study hard regular polygons with the number of edges ranging from 3 to 12. The polygons interact purely entropically due to volume exclusion (steric hindrance)^{3,38,39} and exhibit a rich phase behavior. In particular, they exhibit a sizable portion of possible molecular and colloidal phase behaviors, despite being so simple. In this study, all polygons have the same circumscribed circle of diameter σ . Dimensionless pressure P is defined as $P^* = \beta P \sigma^2$, where β is the inverse of temperature T. We use n-gon as a shorthand for the polygon name, where n is the number of edges.

NPT Monte Carlo (MC) simulations with N identical polygons were performed with the HOOMD-blue software package 40,41 using the HPMC (Hard Particle Monte Carlo) module. 42 The number of polygons and the pressure are fixed, and the system was equilibrated by proposing and accepting or rejecting trial moves where particles are translated or rotated slightly, or the size and shape of the simulation box is changed. The size and shape of the box is allowed to fluctuate so any crystal system can be commensurate with the simulation boundaries. All simulations are run with periodic boundary conditions, and the temperature is fixed such that $k_BT = 1$, but its value does not determine the phase behavior of these hard particle systems. We obtained dense packings by numerically compressing unit cells43,44 containing up to 8 polygons from $P^* = 1$ to $P^* = 10^8$ using an exponential protocol over 3×10^6 MC sweeps. One sweep consists of a trial rotation or translation proposed for each of the N particles and a resize or shear trial move for the box. As expected, equilateral triangles (3-gon) and squares (4-gon) form space-filling tilings in a triangular lattice and a square lattice, respectively. For polygons

with more than four sides, the number of sides determines the plane group of the dense packings. ⁴⁵ Polygons with a number of sides that is neither a multiple of 2 nor 3, i.e., pentagons (5-gon), heptagons (7-gon) and hendecagons (11-gon), form packings with plane group p2mg. Polygons with a number of sides that is a multiple of 2 but not 3, i.e., octagons (8-gon) and decagons (10-gon), form packings with plane group c2mm. The polygon with a number of sides that is a multiple of 3 but not 2, i.e., the nonagons (9-gon), forms a packing with plane group p2. Polygons with a number of sides that is both a multiple of 2 and 3, i.e., hexagons (6-gon) and dodecagons (12-gon), form ordered dense packings with plane group p6mm. The packing fraction, plane group and unit cell parameters of the dense packings are summarized in Table 1.

Systems with N=4000 polygons were initialized in their dense packings and equilibrated by expanding the system to lower pressures in the fluid range, to identify phase transitions by the presence of discontinuities, kinks, or other anomalies in the equations of state. For the polygons demonstrating a crystal to plastic crystal transition in the expansion runs, we identified any hysteresis in the equations of state that would indicate the first order nature of the phase transition by initializing these systems in their plastic crystal phase and equilibrating by compressing to higher pressures. We used 2×10^6 MC sweeps per particle to equilibrate the systems and took measurements in the subsequent 2×10^6 sweeps.

We quantify the tendency for edge alignment by calculating the directional entropic forces using the potential of mean force and torque (PMFT).37 The PMFT gives the per particle free energy of all other particles as a function of the relative positions and orientations of a single particle pair and thus quantifies the effective pairwise free energy of interaction arising from the multi-body entropic effects in the system. We define a coordinate system characterizing pair configurations as θ_1 , θ_2 , and r (Fig. 1). The quantity r is defined to be the magnitude of the vector \mathbf{r}_{12} pointing from the centroid of the first particle to the centroid of the second particle. θ_1 is defined as the angle between \mathbf{r}_{12} and the orientation of particle \hat{n}_1 . θ_2 is defined as the angle between $-\mathbf{r}_{12}$ and the orientation of particle \hat{n}_2 . This pairwise coordinate system is invariant under global rotation and translation (Fig. 1). We calculated the PMFT and integrated r over the range of the first neighbor shell to quantify the directional entropic

Table 1 Putative dense packing structures and plastic crystal properties. Packings are characterized by packing fraction η and plane group. a_1 and a_2 are lattice constants. γ is the unit cell angle. If they exist, plastic crystals are characterized by hysteresis at the plastic crystal–crystal transition and the probability distribution of polygon orientations $P(\theta)$

Polygon	Dense packing structure					Plastic crystal properties		
	Packing fraction η	Plane group	a_1	a_2	γ	Existence	Hysteresis	$P(\theta)$
5	0.92131	p2mg	0.9045	1.4266	90°	Y	Y	Uniform
6	1	p6mm	0.8660	1.5000	90°	N	_	_
7	0.89269	p2mg	0.9505	1.6125	90°	Y	Y	Uniform
8	0.90616	c2mm	0.9239	1.6892	90°	Y	Y	Trimodal
9	0.90103	<i>p</i> 2	0.9776	1.6419	89.52°	Y	Y	Bimodal
10	0.91372	c2mm	0.9511	1.6910	90°	Y	Y	Trimodal
11	0.90766	p2mg	0.9797	1.6719	90°	Y	Y	Uniform
12	0.92820	p6mm	0.9659	1.673	90°	N	_	_

Soft Matter Paper

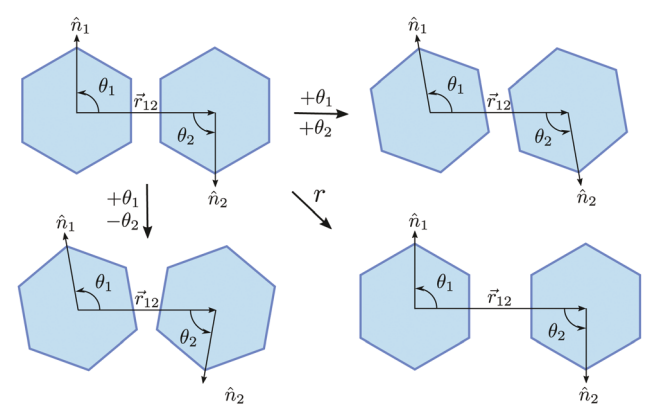


Fig. 1 Pair configuration in two-dimensional systems of anisotropic particles. Pair configurations can be expressed in terms of three scalar quantities (r, θ_1, θ_2) that are invariant under global translations and rotations

forces. The resulting PMFT is the effective entropic interaction of a pair of particles with relative orientations θ_1 and θ_2 , having integrated over all other particles. Importantly, the PMFT by construction is isotropic if particles rotate freely and independently, and anisotropic if orientational correlations are present.

To detect plastic crystal to crystal phase transitions, we calculate equations of state for each n-gon and identify phase transitions by the presence of discontinuities, kinks, and other anomalies in the data. We quantify the development of orientational order as pressure increases using the particle orientational order parameter

$$\Phi_m = \frac{1}{N} \left| \sum_{j=1}^N e^{im\theta_j} \right|. \tag{1}$$

Here θ_i is the orientation of the *j*-th particle and *m* is the least common multiple of the number of polygon edges and the coordination number of its solid. The definition of m removes orientational degeneracies. We quantify the orientational ordering of the plastic crystal phases by calculating the probability distribution of polygon orientations $P(\theta)$. $P(\theta)$ is obtained by constructing a histogram of the orientations of polygons with the redundancy due to polygon symmetry removed.

The correlation of particle orientations as a function of distance is calculated using the correlation function

$$C_{\phi}(r) = \frac{\sum_{l=1}^{N} \sum_{j=1}^{N} e^{ik(\theta_{j} - \theta_{l})} \delta(r - |\mathbf{r}_{l} - \mathbf{r}_{j}|)}{\sum_{l=1}^{N} \sum_{j=1}^{N} \delta(r - |\mathbf{r}_{l} - \mathbf{r}_{j}|)}.$$
 (2)

Here the multiplying factor k is used to account for particle orientational symmetry. For polygons with even number of edges, k equals the number of edges. For polygons with odd numbers of edges, k is twice the number of edges since two polygons with odd number of edges in a face-to-face alignment will be antiparallel to each other. In any plastic crystal, the correlation function $C_{\phi}(r)$ should decay exponentially at sufficiently large distances.

Results

Based on the equations of state, PMFTs, particle orientation distribution functions and orientational order parameter plots we find three distinct overall phase behaviors: 3-, 4-, 6-, and 12-gons have no plastic crystal phase, 5-, 7-, and 11-gons have an indiscrete plastic crystal phase with no preferred orientations, and 8-, 9-, and 10-gons have a discrete plastic crystal phase with preferred orientations. All observed plastic crystal phases have p6mm symmetry and transition to a non-plastic crystal phase with lower symmetry. Details of the three types of phase behaviors follow.

1. No plastic crystal phase

The results for 3-, 4-, 6-, and 12-gons are presented in Fig. 2. Panels (a-d) show representative snapshots of the systems with particles colored by $e^{in\theta}$, where θ is the orientation with respect to the x-axis. The homogeneity of the color in the images shows long-range ordering in the particle orientations. Panels (e-h) show probability distributions of particle orientation; here we reduce the orientation range to the region $[0,2\pi/n]$ for each n-gon to remove degeneracy due to polygon symmetry. A single peak exists in each case (for triangles, $\theta = 0$ and $\theta = \pi$ are the same due to their honeycomb lattice unit cell with anti-aligned particles), showing that there is only one preferred orientation (with thermal fluctuations) for each of these shapes, as would be expected for a crystal. Panels (i-l) show that the particle orientations are correlated over long ranges (using eqn (2)), also as would be expected for a crystal. The PMFTs for 3-, 4-, 6-, and 12-gons have one isolated region of high entropy (free energy minimum) (Fig. 2m-p), indicating there is one entropically preferred local alignment of the particles (disregarding indistinguishable symmetric rotations).

These four polygons have only one anomaly in their equations of state and all appear at low pressure $P^* < 30$ (Fig. 2q). For these and all other n-gons except the 5-gon, the fluid prior to the fluidsolid transition is a hexatic fluid. 46 The hexatic is an anisotropic fluid phase with no translational order, and it appears between the fluid and the solid (plastic crystal or crystal) if it exists. Here, we focus not on that transition, but on the features of the solid phase. 3-, 4-, 6-, and 12-gons develop orientational order (using eqn (1)) already at low pressure immediately following the fluidsolid transition (Fig. 2r). All of these measured quantities show that 3-, 4-, 6-, and 12-gons have only a crystal phase, which is consistent with prior simulation studies that showed 3- and 4-gons do not have a plastic crystal phase. 30,34,35

2. Indiscrete plastic crystal phase

The results for 5-, 7-, and 11-gons are presented in Fig. 3. Panels (a-c) show representative snapshots of the systems. The local randomization of color with no extended patches of color indicate that the polygons are orientationally disordered, despite being translationally ordered. The probability distributions of particle orientation shown in panels (d-f) are uniform in each case, consistent with the snapshot images, and panels (g-i) show that the particle orientations are uncorrelated beyond the first neighbor shell at most. All of this is consistent with an indiscrete plastic Paper Soft Matter

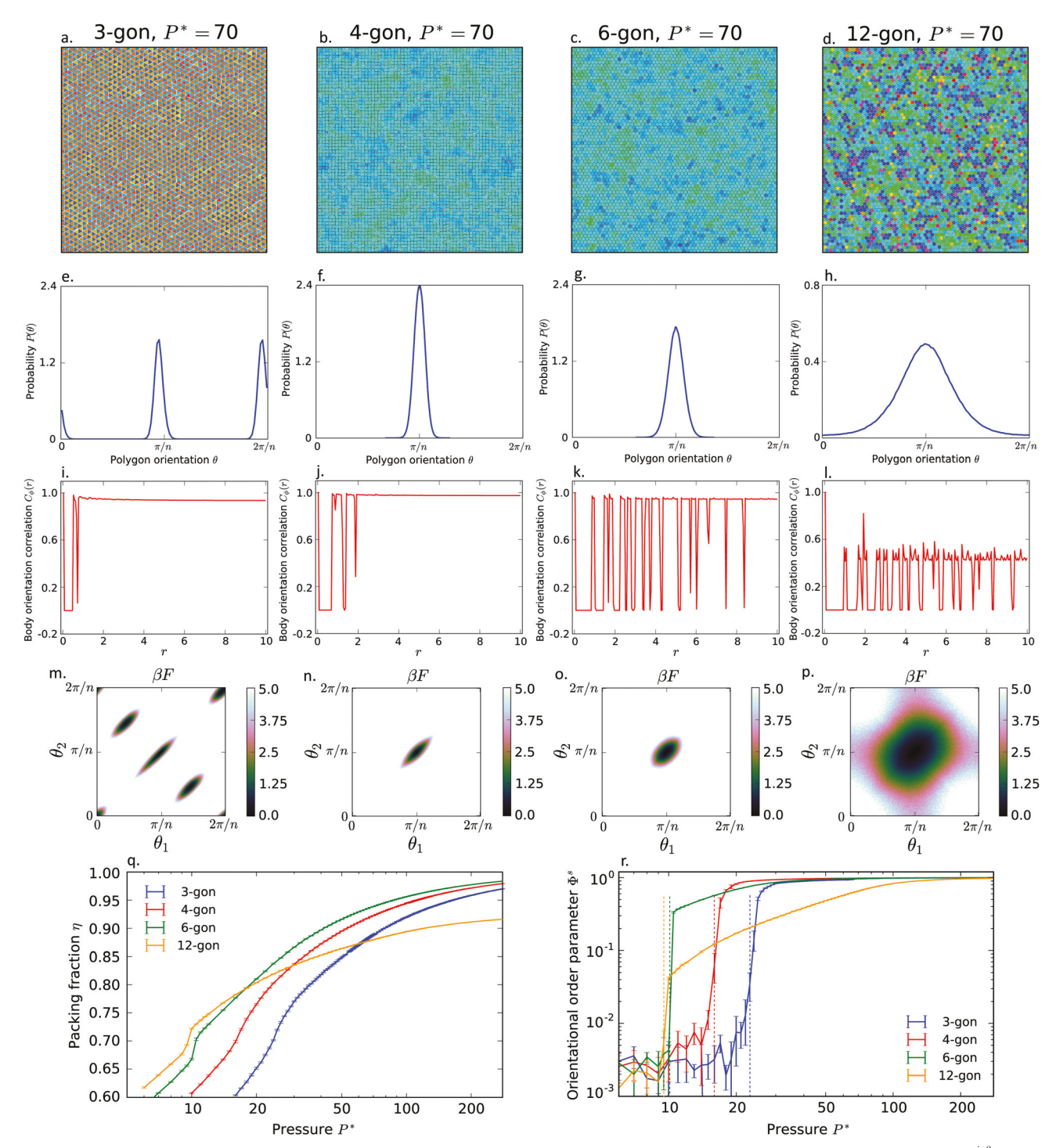


Fig. 2 Characteristics of the phases of 3-, 4-, 6-, and 12-gons. Panels (a-d) are representative snapshots of the systems with particles colored by $e^{in\theta}$, where θ is the orientation with respect to the x-axis, showing long-range orientational ordering. Panels (e-h) are probability distributions of particle orientation. Panels (i-l) plot the particle orientation correlation function (eqn (2)). Panels (m-p) are the PMFTs where θ_1 and θ_2 are defined in Fig. 1. The dark green regions indicate low free energy (high entropy). 3-, 4-, 6-, and 12-gons have only one completely isolated low free energy pair configuration (dark green). Panel (q) shows the equations of state (logarithmic scale), demonstrating the absence of plastic crystal crystal transition regions. Error bars indicate one standard deviation from the mean density taken from NPT simulations. Panel (r) shows the orientational order parameter (logarithmic scale) for each shape. 3-, 4-, 6-, and 12-gons develop orientational order already at low pressure directly after the fluid-solid transition. Dashed lines signify phase transition pressures; here each transition is from a fluid phase to the crystal phase, observed from the points of inflection in the equation of state and corroborated in ref. 46.

crystal phase. The PMFTs for 5-, 7- and 11-gons have extended regions of high entropy, with entropy maxima connected by high entropy pathways (Fig. 3j-l). High entropy pathways indicate

neighboring particles can change their relative orientations easily, with no preferred orientation, as supported by the other measured quantities.

Soft Matter Paper

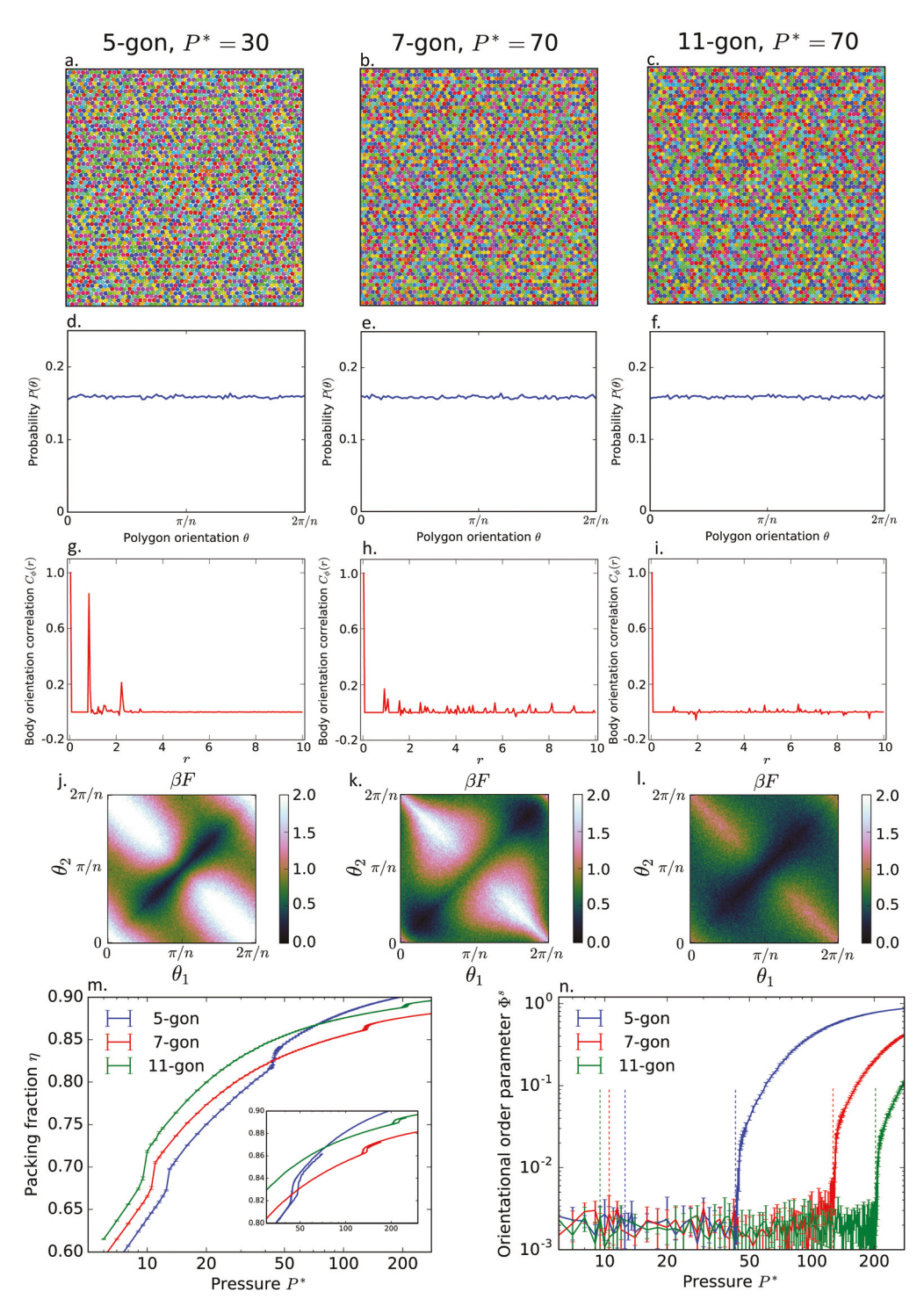


Fig. 3 Characteristics of the phases of 5-, 7-, and 11-gons, laid out as in Fig. 2. System snapshots in panels (a-c) show no detectable preference in the particles' orientations. Orientation distributions in panels (d-f) are uniform. Orientation correlation functions in panels (g-i) demonstrate particles are not correlated over any distance greater than the next nearest neighbor shell. PMFTs in panels (j-l) show that low free energy (high entropy) pair configurations are connected by low free energy pathways, so orientations fluctuate freely. Panel (m) shows the equations of state which show the fluidplastic crystal transition at lower pressures and the plastic crystal-crystal transition at higher pressures. Inset: Enlarged image of the plastic crystal to crystal transition to highlight the slight hysteresis obtained from compression and expansion simulations. The orientation order parameter in panel (n) shows that 5-, 7-, and 11-gons have no orientational order in the plastic crystal prior to the transition to the dense packing structure. The left-most dashed lines indicate the fluid-plastic crystal transition and the right-most dashed lines indicate the plastic crystal-crystal transition.

These polygons exhibit two discontinuities in their equations of state, one at low pressure and another one at high pressure (Fig. 3m). The low-pressure transition connects the hexatic fluid phase (except the 5-gon, for which the fluid is isotropic) to the

Soft Matter **Paper**

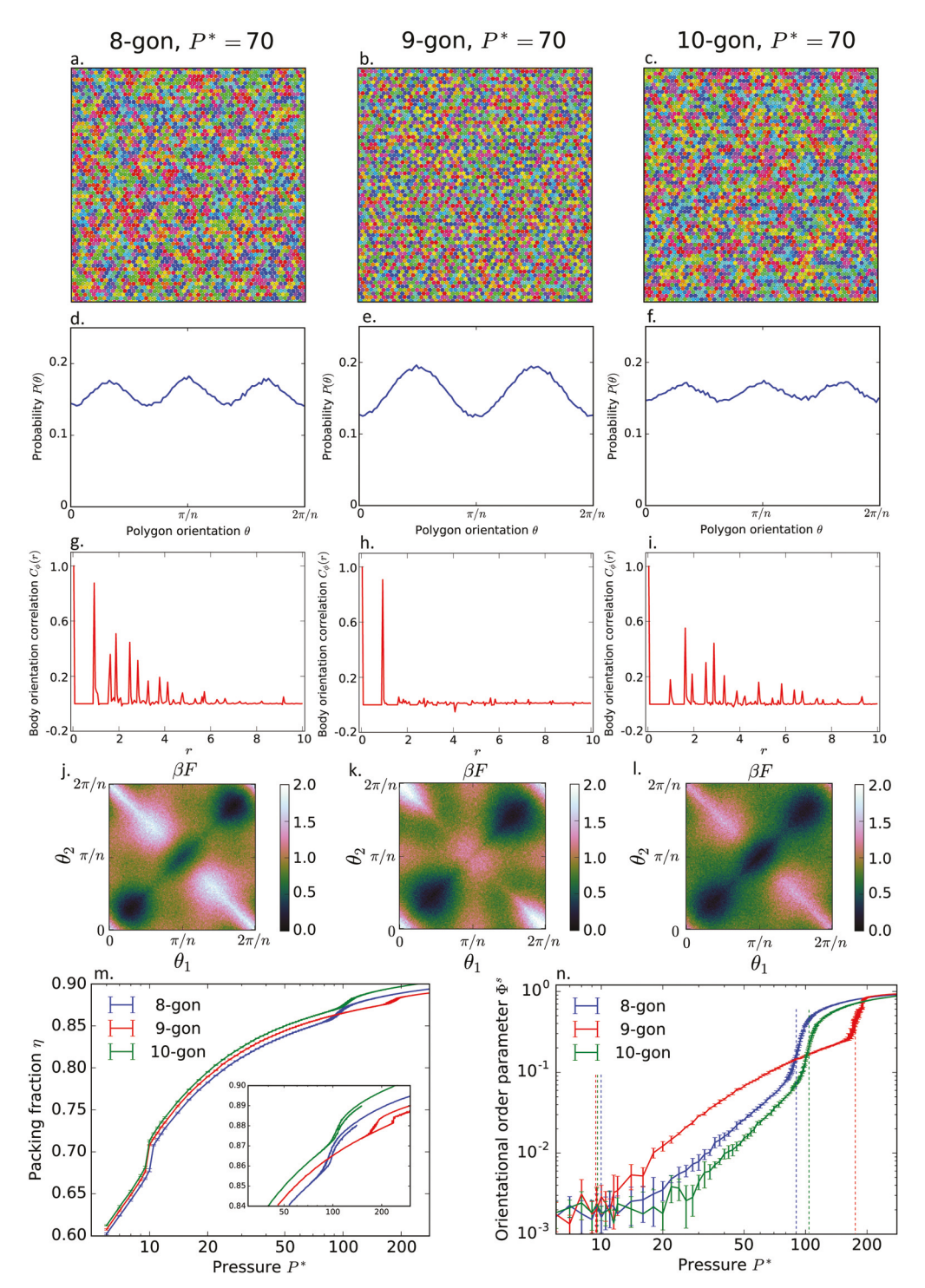


Fig. 4 Characteristics of the phases of 8-, 9-, and 10-gons, laid out as in Fig. 2. System snapshots in panels (a-c) show patches of short-ranged order in the particles' orientations. Orientation distributions in panels (d-f) have multiple peaks, demonstrating preferred particle orientations. Orientation correlation functions in panels (q-i) demonstrate particles are correlated over longer distances than for 5-, 7-, and 11-gons (Fig. 3g and h), but are exponentially decreasing, indicating no long-ranged order. PMFTs in panels (j-l) show that low free energy (high entropy) pair configurations are isolated by high free energy configurations. 8- and 10-gons have three isolated low free energy configurations (j and l) whereas the 9-gons have two. Panel (m) shows the equations of state, which show the fluid-plastic crystal transition at lower pressures and the plastic crystal-crystal transition at higher pressures. Inset: Blow-up of the plastic crystal-crystal transition to highlight the slight hysteresis obtained from compression and expansion simulations, also observed for 5-, 7- and 11-gons (Fig. 3m). The orientation order parameter in panel (n) shows that 8-, 9-, and 10-gons have steadily increasing orientational order in the plastic crystal prior to the transition to the dense packing structure, where it jumps to a larger value. The left-most dashed lines indicate the fluid-plastic crystal transition and the right-most dashed lines indicate the plastic crystal-crystal transition.

Soft Matter

hexagonal plastic crystal phase, and the high-pressure transition connects the plastic crystal phase to the crystal phase. Calculations of the orientational correlation function show vanishing correlations at long range, consistent with the definition of a plastic crystal phase. We find that the transitions from indiscrete plastic crystal to crystal are first order due to the presence of hysteresis in the equation of state curves obtained through compression and expansion runs (Fig. 3m inset).31 Due to the presence of defects and grain boundaries caused by compression, the packing fraction obtained via compression runs tends to be lower than the packing fraction obtained via expansion runs in the dense packing structure region. 5-, 7-, and 11-gons have no orientational order in the plastic crystal phase prior to the transition to the crystal phase; the values of Φ_m in (Fig. 3n) are consistent with the amplitude of thermal noise expected in systems of this size with no orientational order. Taken together, this evidence shows that 5-, 7-, and 11-gons have an intermediate indiscrete plastic crystal phase with no preferred orientations, which agrees with a previous simulation study on 5- and 7-gons by Schilling.31

3. Discrete plastic crystal phase

The results for 8-, 9-, and 10-gons are presented in Fig. 4. Panels (a-c) show representative snapshots of the systems. Local patches of color are larger than for the previous group of polygons, but are still disordered, indicating that these polygons are also orientationally disordered, despite being translationally ordered. Additionally, the orientational correlation function in panels (g-i) vanish at large r as observed for the 5-, 7-, and 11-gons. However, here the probability distributions of particle orientation (panels (d-f)) show multiple peaks, demonstrating three preferred orientations for 8- and 10-gons, and two preferred orientations for 9-gons. All of this is consistent with a plastic crystal phase that is only partially ordered, which we term a discrete plastic crystal phase. This conclusion is supported by calculations of the PMFTs in (Fig. 4j-l). The PMFTs for the 8- and 10-gon have three entropy maxima (shown as free energy minima) connected by low entropy (high free energy) pathways, and the PMFT for the 9-gon has two entropy maxima connected by low entropy pathways. These plots indicate that there are clear entropic preferences in terms of local orientation relative to the lattice, and that these entropic preferences align with the particle orientation probability distribution. The existence of pathways between preferred orientations, even if low entropy (high free energy), means the particles can rotate among the preferred orientations. Fig. 5 and 6 show the most and least preferred particle orientations for 8-gons and 9-gons respectively. We note that multipeaked orientational distributions have also been reported in simulations of hard dumbbells^{9,12} and hard truncated cubes.¹⁴

These three shapes have two discontinuities in their equations of state, one at low pressure and another one at high pressure (Fig. 4m). The presence of hysteresis in all three equations of state indicates the plastic crystal to crystal transitions are all first order (Fig. 4m inset). Fig. 4n shows that 8-, 9-, and 10-gons develop orientational order steadily in the plastic crystal phase up to the transition to the crystal phase, where Φ_m jumps to a high value.

Table 1 summarizes the main results together with characteristics of the lattices. All of the observed behavior can be

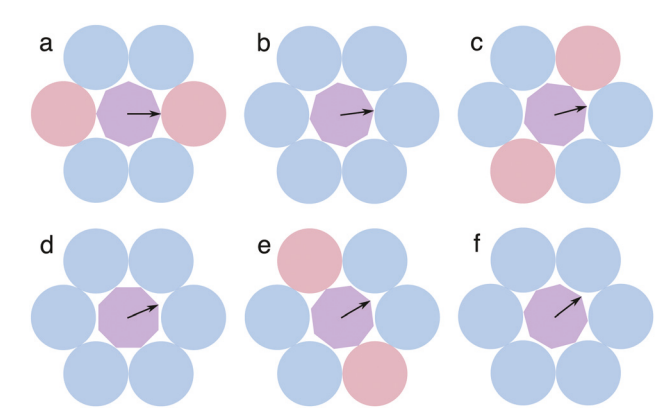


Fig. 5 Local environments of 8-gons in their discrete plastic crystal phase. Nearest neighbor particles are represented schematically with disks. Panels (b-f) are generated from panel (a) by successive rotations of the central 8-gon counterclockwise by $\pi/24$. Panels (a, c, and e) display the least preferred orientations, and panels (b, d, and f) display the most preferred orientations in correspondence with Fig. 4d. Panels (a, c, and e) are unfavorable configurations because of the vertex-centered bonds formed between the central particles and the neighbor particles colored pink. Under successive counterclockwise rotations of $\pi/3$ which leave the surrounding particles invariant, panel (a) transforms into panel (c), then into panel (e), and then back to (a), and panel (b) transforms into panel (d) into panel (f) back into panel (b). This schematic also represents 10-gons because 10-gons have the same form of particle orientation distribution as 8-gons.

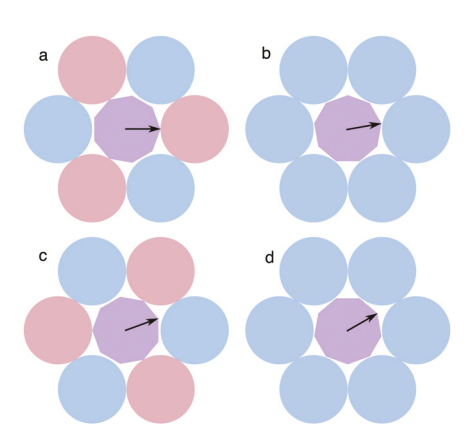


Fig. 6 Local environments of 9-gons in their discrete plastic crystal phase. Nearest neighbor particles are represented schematically with disks. Panels (b-d) are generated from panel (a) by successive rotations of the central 9-gon counterclockwise by $\pi/18$. Panels (a and c) display the least preferred orientations, and panels (b and d) display the most preferred orientations in correspondence with Fig. 4e. Panels (a and c) are unfavorable configurations because of the vertex-centered bonds formed between the central particles and the neighbor particles colored pink. Under successive counterclockwise rotations of $\pi/3$ which leave the surrounding particles invariant, panel (a) transforms into panel (c) back into (a), and panel (b) transforms into panel (d) back into panel (b).

rationalized by comparing the polygon symmetry to the symmetry of the local environment in the solid phase. For 3-, 4-, 6-, and 12-gons, their shape symmetry group contains the symmetry group of their local environment. Consequently, these polygons can easily maximize entropy by aligning neighboring edges; they do not need to rotate to be compatible with the crystal structure,

Paper Soft Matter

which leads to the absence of any plastic crystal phase. For 5-, 7-, 8-, 9-, 10-, and 11-gons, the particle symmetry group does not contain the C_6 symmetry of the hexagonal plastic crystal phases observed for these polygons. Thus edge alignment in these systems is not simple, and entropy maximization cannot be achieved through edge alignment alone. Consider 8- and 10-gons. Because they share a C2 symmetry element with the plastic crystal, they preferentially align in three equally spaced orientations to add the missing C_3 symmetry. The result is a trimodal distribution of particle orientations, effectively recovering the C_6 symmetry of the plastic crystal phase. Similarly, 9-gons share C_3 symmetry elements with the plastic crystal phase but lack a C_2 symmetry, resulting in a bimodal distribution of particle orientations. In contrast, 5-, 7-, and 11-gons share no common nontrivial symmetry elements with the plastic crystal, and so have a plastic crystal phase with no preferred orientations. These polygons are maximally frustrated, and so maximize their entropy by maximizing their rotational degrees of freedom.

Discussion

We have shown that the appearance of plastic crystal phases can indeed be ascribed to the tendency of particles to orient themselves to be compatible with their local environment, as previously hypothesized.²³⁻²⁸ We have shown that this compatibility is achieved by matching symmetries to maximize entropy. Our results reveal a general pattern relating the number of edges of regular polygons to all aspects of their plastic crystal phase behavior. Based on this pattern, we identify the relationship between the symmetry group G of a particle and the symmetry group H of the local environment of the solid phase as the dominating factor producing the plastic crystal phase. Our findings may be summarized in the following three rules:

Rule 1. If H is a subgroup of G, then a plastic crystal is absent. Rule 2. If G shares some but not all nontrivial symmetry elements with H, then a discrete plastic crystal phase is present which has preferred orientations that recover the missing symmetry elements.

Rule 3. If G and H share no nontrivial symmetry elements, then an indiscrete plastic crystal phase is present without preferred particle orientations.

These rules cover all regular n-gons, although the plastic crystal to crystal transitions will appear at increasingly higher pressures and with diminishing signatures. We believe these symmetry considerations will enable the design of new shapes exhibiting plastic crystal phases with targeted particle orientation distributions.

Conflicts of interest

There are no conflicts to declare.

Acknowledgements

We acknowledge helpful discussions with Julia Dshemuchadse, Eric Harper, and Matthew Spellings. We thank an anonymous reviewer for the suggested terminology of "discrete" and "indiscrete" plastic crystal phases. This material is based upon work supported in part by the U.S. Army Research Office Grant Award No. W911NF-10-1-0518, by the National Science Foundation, Division of Materials Research Award # DMR 1409620, and by a Simons Investigator award from the Simons Foundation to S. C. G. J. Antonaglia acknowledges a National Science Foundation Graduate Research Fellowship Grant DGE 1256260. Computational resources and services supported by Advanced Research Computing at the University of Michigan, Ann Arbor.

References

- 1 U. Agarwal and F. A. Escobedo, Nat. Mater., 2011, 10, 230-235.
- 2 P. F. Damasceno, M. Engel and S. C. Glotzer, Science, 2012, 337, 453-457.
- 3 D. Frenkel, Nat. Mater., 2014, 14, 9-12.
- 4 K. Zhao and T. G. Mason, Phys. Rev. Lett., 2009, 103, 208302.
- 5 K. Zhao, R. Bruinsma and T. G. Mason, Proc. Natl. Acad. Sci. U. S. A., 2011, 108, 2684-2687.
- 6 H. R. Vutukuri, A. Imhof and A. van Blaaderen, Angew. Chem., Int. Ed., 2014, 53, 13830-13834.
- 7 M. Baur and K. Huang, Phys. Rev. E, 2017, 95, 030901.
- 8 Z. Hou, K. Zhao, Y. Zong and T. G. Mason, Phys. Rev. Mater., 2019, 3, 015601.
- 9 C. Vega, E. P. A. Paras and P. A. Monson, J. Chem. Phys., 1992, 96, 9060.
- 10 E. G. Noya, C. Vega, J. P. K. Doye and A. A. Louis, J. Chem. Phys., 2007, 127, 054501.
- 11 R. Rey, J. Chem. Phys., 2008, 129, 224509.
- 12 J. L. Aragones, M. M. Conde, E. G. Noya and C. Vega, Phys. Chem. Chem. Phys., 2009, 11, 543-555.
- 13 E. G. Noya, C. Vega, J. P. K. Doye and A. A. Louis, J. Chem. Phys., 2010, 132, 234511.
- 14 A. P. Gantapara, J. de Graaf, R. van Roij and M. Dijkstra, J. Chem. Phys., 2015, 142, 054904.
- 15 Z. Hou, Y. Ju, Y. Zong, F. Ye and K. Zhao, Chin. Phys. B, 2018, 27, 088203.
- 16 S. C. Glotzer and M. J. Solomon, Nat. Mater., 2007, 6, 557-562.
- 17 G. van Anders, D. Klotsa, A. S. Karas, P. M. Dodd and S. C. Glotzer, ACS Nano, 2015, 9, 9542-9553.
- 18 S. Long, D. R. MacFarlane and M. Forsyth, Solid State Ionics, 2003, 161, 105-112.
- 19 J. N. Sherwood, Mol. Cryst., 1969, 9, 37-57.
- 20 R. Aronsson, J. Chem. Phys., 1982, 77, 677.
- 21 L. Börjesson and L. M. Torell, Phys. Rev. B: Condens. Matter Mater. Phys., 1985, 32, 2471-2477.
- 22 D. R. MacFarlane, P. Meakin, N. Amini and M. Forsyth, J. Phys.: Condens. Matter, 2001, 13, 8257-8267.
- 23 F. Simon and C. v. Simson, Z. Phys., 1924, 21, 168-177.
- 24 L. Pauling, Phys. Rev., 1930, 36, 430-443.
- 25 H. M. James and T. A. Keenan, J. Chem. Phys., 1959, 31, 12.
- 26 L. Staveley, J. Phys. Chem. Solids, 1961, 18, 46-52.
- 27 J. Timmermans, J. Phys. Chem. Solids, 1961, 18, 1-8.
- 28 W. Dunning, J. Phys. Chem. Solids, 1961, 18, 21-27.

29 L. Onsager, Ann. N. Y. Acad. Sci., 1949, 51, 627-659.

Soft Matter

- 30 K. W. Wojciechowski and D. Frenkel, *Comput. Methods Sci. Technol.*, 2004, **10**, 235–255.
- 31 T. Schilling, S. Pronk, B. Mulder and D. Frenkel, *Phys. Rev. E: Stat., Nonlinear, Soft Matter Phys.*, 2005, **71**, 036138.
- 32 J. de Graaf, R. van Roij and M. Dijkstra, *Phys. Rev. Lett.*, 2011, **107**, 155501.
- 33 J. A. Millan, D. Ortiz, G. van Anders and S. C. Glotzer, ACS Nano, 2014, 8, 2918–2928.
- 34 C. Avendaño and F. A. Escobedo, Soft Matter, 2012, 8, 4675.
- 35 A. P. Gantapara, W. Qi and M. Dijkstra, *Soft Matter*, 2015, **11**, 8684–8691.
- 36 P. F. Damasceno, M. Engel and S. C. Glotzer, *ACS Nano*, 2012, **6**, 609–614.
- 37 G. van Anders, D. Klotsa, N. K. Ahmed, M. Engel and S. C. Glotzer, *Proc. Natl. Acad. Sci. U. S. A.*, 2014, **111**, E4812–E4821.

- 38 M. Dijkstra, *Advances in Chemical Physics*, John Wiley & Sons, Inc., 2014, vol. 156, pp. 35–71.
- 39 V. N. Manoharan, Science, 2015, 349, 1253751.
- 40 J. A. Anderson, C. D. Lorenz and A. Travesset, *J. Comput. Phys.*, 2008, 227, 5342–5359.
- 41 J. A. Anderson, E. Jankowski, T. L. Grubb, M. Engel and S. C. Glotzer, *J. Comput. Phys.*, 2013, **254**, 27–38.
- 42 J. A. Anderson, M. Eric Irrgang and S. C. Glotzer, *Comput. Phys. Commun.*, 2016, **204**, 21–30.
- 43 E. R. Chen, M. Engel and S. C. Glotzer, *Discrete Comput. Geom.*, 2010, 44, 253–280.
- 44 L. Filion, M. Marechal, B. van Oorschot, D. Pelt, F. Smallenburg and M. Dijkstra, *Phys. Rev. Lett.*, 2009, **103**, 188302.
- 45 Y. L. Duparcmeur, A. Gervois and J. Troadec, *J. Phys. I*, 1995, 5, 1539–1550.
- 46 J. A. Anderson, J. Antonaglia, J. A. Millan, M. Engel and S. C. Glotzer, *Phys. Rev. X*, 2017, 7, 021001.